



1 **Dynamic-Statistic Combined Ensemble Prediction and** 2 **Impact Factors on China's Summer Precipitation**

3 Xiaojuan Wang¹, Zihan Yang^{2*}, Shuai Li³, Qingquan Li³, Guolin Feng^{3,4*}

4 1 College of Electronic and Information Engineering, Changshu Institute of Technology, Suzhou,
5 215506, China

6 2 Department of Atmospheric Sciences, Yunnan University, Kunming, 650500, China

7 3 Laboratory for Climate Research, National Climate Center, Beijing, 100081, China

8 4 College of Physical Science and Technology, Yangzhou University, Yangzhou, 225009, China

9
10 **Abstract** The dynamic-statistic prediction shown excellent performance on monthly
11 and seasonal precipitation prediction in China and has been applied on several
12 dynamical models. In order to further improve the prediction skill of summer
13 precipitation in China, the Unequal-Weighted Ensemble prediction (UWE) based on
14 the dynamic-statistic combined schemes is presented, and its possible impact factors
15 are also analyzed. Results indicate that the UWE has shown promise in improving the
16 prediction skill of summer precipitation in China, on account to the UWE can
17 overcome shortcomings of the structural inadequacy of individual dynamic-statistic
18 prediction, reducing formulation uncertainties, resulting in more stable and accurate
19 predictions. Impact factors analysis indicates that 1) the station-based ensemble
20 prediction with ACC being 0.10-0.11 add PS score being 69.3-70.2, has shown better
21 skills than the grid-based one, as the former produces probability density distribution
22 of precipitation being closer to the observation than the latter. 2) The use of the spatial
23 average removed anomaly correlation coefficient (SACC) may lower the prediction
24 skill and introduce obvious errors on estimating the spatial consistency of prediction
25 anomalies. SACC could be replaced by the revised anomaly correlation coefficient
26 (RACC), which is calculated directly using the precipitation anomalies of each station
27 without subtracting the average precipitation anomaly of all stations. 3) The low
28 dispersal intensity among ensemble samples of UME implies the historical similar
29 error selected by different approach is quite close to each other, making the correction
30 on the model prediction is more reliable. Therefore, the UWE is expected to further
31 improve the accuracy of summer precipitation prediction in China by considering
32 impact factors such as the grid



33 or station-based ensemble approach, the method of calculating the ACC, and the
34 dispersal intensity of ensemble samples in the application and analysis process of
35 UWE.

36

37 **Keywords:** Dynamic-statistic prediction, Unequal weighted ensemble prediction,
38 Prediction accuracy, Dispersal intensity, Revised anomaly correlation coefficient

39

40



41 **Introduction**

42 Accurate prediction of summer precipitation across China is paramount for dealing
43 with critical issues such as flood and drought management, economic development,
44 and ensuring food security. However, this task is fraught with challenges due to the
45 intricate interplay among various atmospheric circulation components, including the
46 East Asian summer monsoon (Ding, 1994; Lu, 2005), the Northwest Pacific
47 subtropical high (Tao, 2006), and the East Asia-Pacific teleconnection patterns
48 (Huang, 2004; Huang, 1987). Additionally, external influences, such as the El
49 Niño-Southern Oscillation (ENSO) (Sun et al., 2021) and the snow cover on the
50 Tibetan Plateau (Si and Ding, 2013), further complicate the prediction process. Due to
51 these complexities, increasing the accuracy of summer rainfall prediction in China
52 still faces challenges, the pursuit of more precise summer rainfall predictions in China
53 is an endeavor that warrants the utmost attention from climate scientists (Gong et al.,
54 2016; Wang et al., 2012).

55
56 Over the past few decades, there has been a remarkable progression in the foundation
57 of observational data and theoretical understanding, which has significantly enhanced
58 the capabilities of climate dynamical models in predicting seasonal rainfall
59 (Gettelman et al., 2022; Wu et al., 2017). High-resolution climate simulations, such as
60 those with atmospheric resolutions of approximately 50 km and oceanic resolutions of
61 0.25°, have been successfully implemented by several research institutions (Roberts et
62 al., 2016; Satoh et al., 2014; Wu et al., 2021). These dynamic models have also
63 demonstrated success in long-term prediction of atmospheric circulation patterns and
64 sea surface temperatures in low-latitude regions (Zhu and Shukla, 2013). However,
65 the current performance of seasonal predictions for key climate elements, including
66 rainfall and temperature, particularly in monsoon-influenced areas like East Asia
67 (Gong et al., 2017; Wang et al., 2015), remains somewhat constrained due to inherent
68 limitations in parameterization schemes and the challenges associated with boundary
69 value problems (Wang et al., 2015). This has spurred meteorologists to delve deeper
70 into understanding how to effectively enhance the seasonal prediction skills of climate
71 models to better align with the needs of end-users (Gong et al., 2016). It is well
72 recognized that regional climate characteristics can significantly influence local
73 rainfall patterns. Despite this, dynamic models still struggle to accurately capture
74 these nuances, suggesting that there is potential for improvement in rainfall prediction



75 through a statistical-dynamic approach (Specq and Batté, 2020). This integrated
76 methodology could provide a more robust framework for prediction, ultimately
77 leading to more reliable and actionable climate predictions.

78

79 To enhance the precision of rainfall prediction, Chou (1974) initially suggested the
80 integration of dynamical model data with statistical analogue information. This
81 approach leverages the prediction errors from historical years with analogous initial
82 conditions, such as similar circulation anomalies, snow cover, and sea surface
83 temperatures (SST), to refine dynamic-analogue correction techniques. For instance,
84 Huang et al. (1993) introduced the evolutionary analogue-based multi-time prediction
85 method, (Ren and Chou, 2006; Ren and Chou, 2007) employs historical analogue data
86 to estimate model errors in accordance with the atmospheric analogy principle, (Feng
87 et al., 2020; Feng et al., 2013) further develops this concept with their correction
88 method focused on key regional impact factors. Wang and Fan (2009) proposed a
89 scheme that integrates model forecasts with the observed spatial patterns of historical
90 "analog years," while Gong et al. (2018) advanced the leading mode-based correction
91 method. In addition to these advancements, dynamic-statistic correction methods have
92 been successfully applied to rainfall predictions in regions such as North China (Yang
93 et al., 2012) and Northeast China (Xiong et al., 2011b). Furthermore, the application
94 of these dynamic-statistic prediction has been extended to seasonal predictions,
95 including those for autumn, winter, and spring (Lang and Wang, 2010). At the Beijing
96 Climate Center, various error selection methods have been operationalized in rainfall
97 prediction, including the raw field-based similar error selection method, the empirical
98 orthogonal function-based similar error selection method, the grid-based similar error
99 selection method, the regional key impact factors-based similar error selection method,
100 and the abnormal factor-based similar error selection method (Feng et al., 2020).
101 These innovative approaches underscore the ongoing efforts to harness both
102 dynamical and statistical insights to achieve more accurate and reliable rainfall
103 predictions.

104

105 Research has consistently demonstrated the benefits of integrating predictions from
106 multiple climate models. For instance, the Bayesian model averaging approach (Luo
107 et al., 2007) and the moving coefficient ensemble approach (Yang et al., 2024) are
108 two such approaches that have shown promise. The use of a multi-model ensemble



109 can mitigate the collective local biases that can occur in space, time, and across
110 different variables when using individual models (Krishnamurti et al., 2016). This
111 approach not only assigns higher weights to the outputs of more accurate models but
112 also enhances overall predictive skill and reduces the uncertainty associated with
113 single-model ensembles (Yan and Tang, 2013). By accounting for comprehensive
114 uncertainties stemming from both model discrepancies and initial conditions,
115 multi-model ensembles often outperform single models (Palmer et al., 2004).
116 Furthermore, the diverse assumptions inherent in different model frameworks can
117 potentially compensate for our incomplete understanding of atmospheric dynamics
118 (Yan and Tang, 2013). The multi-model approach has been successfully applied
119 across a broad spectrum of forecasting needs, including medium-range weather
120 forecasting (Candille, 2009) and seasonal climate prediction (Vitart, 2006). Given the
121 aforementioned advantages of dynamic-statistic methods in seasonal predictions, it is
122 imperative to adopt an ensemble approach that combines the predictions from these
123 methods. This integration is crucial for further enhancing prediction accuracy and
124 reliability. By leveraging the collective strengths of various models and techniques,
125 we can achieve a more robust and nuanced understanding of climate patterns,
126 ultimately leading to improved prediction capabilities.

127

128 In the process of examining the ensemble prediction, it is crucial to take into account
129 the various factors that can influence its predictive accuracy (Krishnamurti and
130 Kumar, 2012). The ensemble's output is particularly sensitive to several key elements:
131 the number of models incorporated, the duration of the dataset utilized for training,
132 and the distribution of weights for both downscaling and the integration of multiple
133 models or schemes (Krishnamurti et al., 2016). Both grid-based reanalysis data and
134 station-based observational data can serve as the foundation for model training or
135 validation (Ding et al., 2004; Gong et al., 2016; Wang et al., 2015). It is therefore
136 essential to explore and discuss the differential impact that the use of these two
137 distinct types of datasets may have on ensemble predictions. Furthermore, the
138 dispersion of samples across different models or methodologies cannot be overlooked,
139 as it also affects the ensemble's predictive skill, and deserve certain attention (Houze
140 et al., 2015).

141

142 Based on above statement, the aim of this research is to construct an



143 Unequal-Weighted Ensemble prediction (UWE) employing a comprehensive array of
144 dynamic-statistic methods and to explore the potential factors that may influence its
145 predictive capabilities. Specifically, the study is designed to delve into three primary
146 areas: (1) Elucidate the process of establishing the UWE through a suite of
147 dynamic-statistic methods, highlighting the distinctions between grid-based
148 ensembles and station-based ensembles. (2) Examine the most effective
149 methodologies for evaluating the spatial congruence between observational data and
150 the UWE's output. (3) Investigate the connection between the dispersal of samples
151 across various dynamic-statistic methods and the predictive accuracy of the UWE.
152 This study will provide a comprehensive analysis of the UWE's development and its
153 performance, offering valuable insights into the factors that influence its predictive
154 success.

155

156 **1 Data and Method**

157 **1.1 Data**

158 The monthly precipitation data of 1634 stations during 1983–2020 are from the
159 National Meteorological Information Center of the China Meteorological
160 Administration. The monthly grid precipitation data during 1983–2020 is derived
161 from the Combined Rainfall Analysis (CMAP) data of the U.S. Climate Prediction
162 Center. The model prediction data for summer precipitation in China are hindcast
163 datasets of the BCC_CPSv3. Monthly climate indices during 1983–2020 including
164 circulation indices (i.e. AO, AAO), SST indices (i.e. Nino 3.4, Nino 4, Pacific
165 Decadal Oscillation), snow cover indices (i.e. Tibet snow cover area index, Northeast
166 China snow cover area index) is available from the Beijing Climate Center website
167 (http://cmdp.ncc-cma.net/Monitoring/cn_index_130.php) (Gong et al., 2016).

168 **1.2 Climate regions division**

169 Climate in China influence by various climate systems, such as the Monsoon,
170 mid-high latitude circulation system and westly jet circulation system etc. (Ding, 1994;
171 Li et al., 2008; Wu et al., 2017). Since summer rainfall has regional characteristics
172 and potential impact factors, we divide the whole country into 8 regions (Feng et al.,
173 2020) in terms of South China (110°~120°E, 20°~25°N), East China (110°~123°E,
174 25°~35°N), North China (110°~123°E, 35°~42.5°N), Northeast China (110°~135°E,
175 42.5°~55°N), Eastern Northwest China (90°~110°E, 35°~43°N), Western Northwest
176 China (75°~90°E, 35°~48°N), Tibet Area (80°~100°E, 27°~35°N and Southwest China



177 (95°~110°E, 22°~33°N). Each region is treated separately by the dynamic-statistic
178 prediction process.

179

180 1.3 The dynamic-statistic predictions

181 Numerical model is an approximation of the behavior of the actual atmosphere. The
182 dynamic-statistic prediction is to utilize the information of historical analogues to
183 estimate model's prediction errors through the statistical method, thereby to
184 compensate the model deficiencies and reduce the model errors (Huang et al., 1993).
185 As addressed by Feng et al. (2020), the dynamic-statistic prediction can be explained
186 by equation (1),

$$187 \hat{p}(\psi_0) = p(\psi_0) + \tilde{p}(\psi_j) - p(\psi_j), \quad (1)$$

188 Where $\hat{p}(\psi_0)$ is the corrected prediction, $p(\psi_0)$ is the original model prediction,
189 and $p(\psi_j)$ is the model prediction of historical year having the similar initial
190 conditions as current one, $\tilde{p}(\psi_j)$ is the corresponding historical observation. Eq. (1)
191 is the integral form of the similarity error correction equation, in which the error term
192 of the similar historical prediction $\tilde{p}(\psi_j) - p(\psi_j)$ is added to the prediction results of
193 the numerical model.

$$194 \hat{p}(\psi_0) \xrightarrow{\text{Estimate}} \hat{E}(\psi_0), \quad (2)$$

195 The core idea of the dynamic-statistic prediction is developing the scheme how to
196 select the similar year and estimate historical prediction errors (Feng et al., 2013;
197 Gong et al., 2016). Eq. (2) transforms improvement in the dynamical model prediction
198 into the estimation of model error (Feng et al., 2013; Ren and Chou, 2006; Xiong et
199 al., 2011b).

200

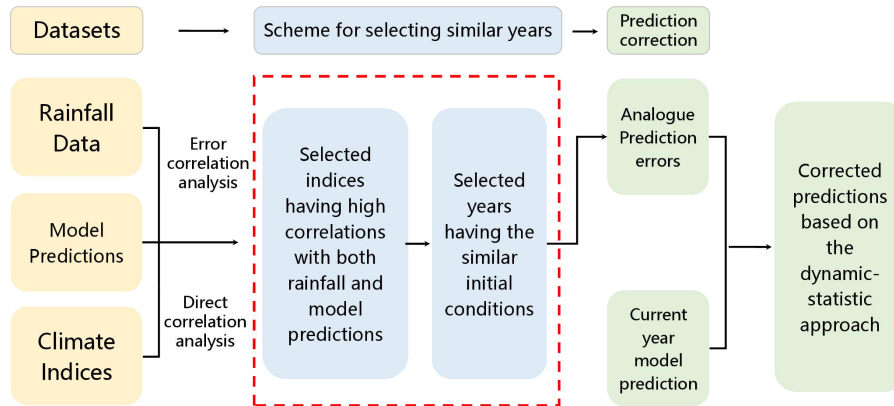
201 1.4 Schemes for the dynamic-statistic prediction

202 Fig.2 presents the flow chart of the dynamic-statistic prediction method. The key step
203 is the scheme for selecting the historical similar years, which is the step in the red box.
204 Different scheme of selecting similar years from the historical dataset corresponds to
205 different dynamic-statistic prediction scheme. In previous years, a series of the
206 dynamic-statistic prediction schemes has been developed for selecting similar years
207 from the historical information, and excellent results have been achieved in predicting
208 summer precipitation anomalies in China (Feng et al., 2013; Wang and Fan, 2009;



209 Wang et al., 2015; Xiong et al., 2011b).

210



211

212 **Fig. 1** The flow chart of the dynamic-statistic prediction method. The key step is the
213 scheme for selecting the historical similar years, which is the step presented in the red
214 dash box.

215

216 Five kinds of the dynamic-statistic prediction approach representing different
217 scheme for analogue error selection are introduced as follows,

218 1) The scheme for original model prediction-based similar error selection (ORM).
219 With the dynamical model original prediction, select four historical years has the most
220 similar feature of anomaly distribution as the current year's prediction. Then calculate
221 the analogue prediction error using these similar years, add to the current prediction
222 and produce the corrected prediction.

223 2) The scheme for Empirical Orthogonal Function mode-based similar error
224 selection (EOF). Calculating the model prediction error filed and produce the
225 corresponding spatial modes and corresponding principal components using the EOF
226 method. Similar years is selected based on the Euclidean distance of the principal
227 components. Historical similar error is calculated using the selected similar years and
228 added to the current model prediction, which then produce the corrected prediction
229 (Gong et al., 2018).

230 3) The scheme for the regional average precipitation-based similar error selection
231 (REG). Dividing the whole country into 8 regions using according to the introduction
232 of section 1.2. Selecting the climate indices having high correlations with the regional
233 average precipitation of each region. With these highly correlated indices,



234 multi-factors are randomly configured and used to calculate the shortest Euclidean
235 distance to choose the historical similar years and produce the similar error.
236 Cross-validation are carried out to correct the model prediction error and obtain the
237 optimal multi-factor configuration. Based on this final optimal multi-predictor
238 configuration, the dynamic-statistic prediction can be implemented (Xiong et al.,
239 2011b).

240 4) The scheme for the grid precipitation-based similar error selection (GRD).
241 The similar error selection is the same as the REG approach, but the model prediction
242 error correction is carried out on each grid point within a region.

243 5) The scheme for the abnormal factors based similar error selection (ABN).
244 Establish factors having significant correlations with the regional precipitation.
245 Determine the anomaly threshold of each factor and select the key factors reaching
246 the threshold. Based on the selected abnormal factors, similar years are selected by
247 the shortest Euclidean Distance of factor set between current year and historical years.
248 Then the analogue errors can be calculated by using the method of weighted average
249 integration and be added on the current year's model prediction, which can produce
250 the corrected prediction (Feng et al., 2020).

251 The selected similar years are not consistent with each other among these five
252 schemes, the analogue errors usually show similar pattern, but have difference in
253 detail. Besides the dynamic-statistic prediction, the system error correction are also
254 presented for comparison.

255

256 1.5 The ensemble for dynamic-statistic prediction

257 Based on the five the dynamic-statistic prediction schemes, the unequal
258 weighting ensemble prediction (UWE) E_m is calculated as equation (3),

$$259 E_m = \sum_{k=1}^n w_{km} F_{km} \quad (n=5) , \quad (3)$$

260 Where F_{km} is the single prediction of each dynamic-statistic scheme and w_{km} is the
261 weight coefficient of each member. n denotes the total number of dynamic-statistic
262 scheme, m denotes the current prediction year. w_k can be calculated using equation
263 (4).

$$264 w_k(i) = \frac{T_k(i)}{\sum_{k=1}^n |T_k(i)|} , \quad (4)$$



265 Where $T_k(i)$ is the correlation coefficients between the dynamic-statistic prediction
 266 and observation at each station or grid point i . One year out validation is
 267 implemented to define weight coefficients. The anomaly correlation coefficient
 268 (ACC), PS score, and root mean standard error are used for evaluating the prediction
 269 skill for summer precipitation in China. The PS score can be calculated using
 270 equation (5).

$$271 \quad PS = \frac{f_0 \times N_0 + f_1 \times N_1 + f_2 \times N_2}{N - N_0 + f_0 \times N_0 + f_1 \times N_1 + f_2 \times N_2 + M} \times 100, \quad (5)$$

272 Where N is the total number of stations, is the number of the correctly predicted
 273 stations with abnormal within (-20%, 20%), f_0 is weight coefficient of N_0 ; N_1 and
 274 f_1 are for the stations with abnormal within (-50%, -20%) or (20%, 50%); N_2 , f_2
 275 are for the stations with abnormal within (-100%, -50%) or (50%, 100%); M is the
 276 total number of correctly predicted stations with abnormal below -100% or above
 277 100%. In this study, we set $f_0 = 2$, $f_1 = 2$ and $f_2 = 4$.

278 Normally, the spatial average removed ACC (SACC) is calculated by formular (6) to
 279 assess the spatial consistency of prediction for summer precipitation in China (Fan et
 280 al., 2012; Xiong et al., 2011b).

$$281 \quad R = \frac{\sum_{i=1}^n (x_i - \bar{x}_s)(y_i - \bar{y}_s)}{\sqrt{\sum_{i=1}^n (x_i - \bar{x}_s)^2 \sum_{i=1}^n (y_i - \bar{y}_s)^2}}, \quad (6)$$

282 Where n is the total number of stations, x_i is the summer precipitation abnormal of
 283 observation at station i , while y_i is the summer precipitation abnormal of prediction
 284 at station i . \bar{x} and \bar{y} are respectively the average abnormal of observation and
 285 prediction for all the stations. This so-called SACC need to subtract the average
 286 precipitation anomaly of all stations from precipitation anomaly of each station before
 287 calculating the ACC.

288 In order to confirm if the SACC can properly estimate the spatial consistency of
 289 prediction for summer precipitation, we also calculated the revised anomaly
 290 correlation coefficient (RACC) using formular (7),

$$291 \quad R^* = \frac{\sum_{i=1}^n (x_i^o - \bar{x}_{i,t})(y_i^o - \bar{y}_{i,t})}{\sqrt{\sum_{i=1}^n (x_i^o - \bar{x}_{i,t})^2 \sum_{i=1}^n (y_i^o - \bar{y}_{i,t})^2}} \quad (7)$$



292 Where n is the total number of stations, x_i^o and y_i^o are respectively the summer
 293 precipitation of observation and prediction at station i . $\bar{x}_{i,t}$ and $\bar{y}_{i,t}$ is the average of
 294 observation and prediction of summer precipitation for all the years at each station i .
 295 The RACC is calculated directly using the precipitation anomalies of each station
 296 without removing the average precipitation anomaly of all stations.

297

298 2 The summer precipitation prediction using the dynamic-statistic scheme

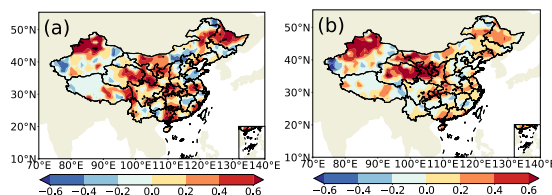
299 The RACCs and PSs of the summer precipitation in China produced by the five
 300 dynamic-statistic methods are presented in Table 1. The 10-year average of PS score
 301 of the dynamic-statistic methods varied from 67.4-69.6, which have the better
 302 performance than that of the SYS method (65.8). In figure 2, the temporal correlation
 303 coefficients of the dynamic-statistic methods are higher than the SYS method over
 304 most China with the distribution spatial pattern is similar to each other, but the most
 305 improved areas varied among different method. It is further confirmed with previous
 306 studies that the merger of prediction error estimated via the statistical method and
 307 dynamic model-based original output represents a potential means for improving
 308 prediction skill of summer rainfall in China (Feng et al., 2020).

309

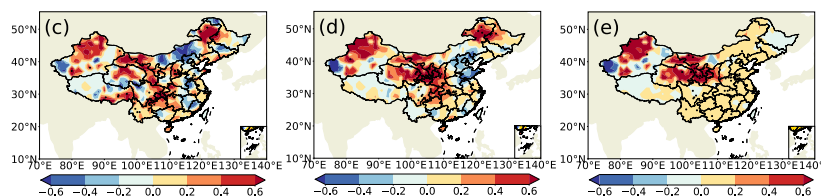
310 **Table 1** 10-year average of RACC and PS of the summer precipitation prediction
 311 from 2011 to 2020 for the dynamic-statistic predictions and system error correction.

Scheme	ORM	EOF	REG
RACC	0.10	0.03	0.01
PS	69.5	69.6	67.4
Scheme	GRD	ABN	SYS
RACC	0.05	0.02	-0.08
PS	68.2	69.4	65.8

312



313



314
 315 **Fig. 2** The differences of the temporal correlation coefficients for summer
 316 precipitation predictions in China from 2011 to 2020. Values indicate differences of
 317 the dynamic-statistic method minus the SYS method. (a) ORM, (b) EOF, (c) REG, (d)
 318 GRD, and (e) ABN.

319
 320 Based on the equation of formular (1), four schemes of UWE prediction using the
 321 single dynamic-statistic predictions as ensemble members and their corresponding
 322 one year out cross validations are presented in Table 2. In order to distinguish the
 323 performances UWE prediction against the grid-point observation and station
 324 observation, both the grid-based ensemble and station-based ensemble are calculated.
 325 Comparing with the single scheme of the dynamic-statistic prediction, the E4 scheme
 326 has the best skill among the four ensemble schemes, with RACC being 0.9 and PS
 327 score being 70. The grid-based ensemble can somewhat improve the summer
 328 precipitation prediction in China, but its effect varied among different schemes. The
 329 skills of the station-based ensemble are obviously better than the grid-based one, with
 330 RACC being 0.10-0.11 add PS score being 69.3-70.2. As addressed by Yan and Tang
 331 (2013) the multi-model ensemble approach (MME) considers the structural
 332 inadequacy of individual models and can reduce model formulation uncertainties. The
 333 reason why the ensemble of multiple dynamic-statistic predictions can improve the
 334 summer precipitation in China is similar to that of MME, which can somewhat
 335 overcome the shortcomings of a single prediction and produce the more stable
 336 prediction.

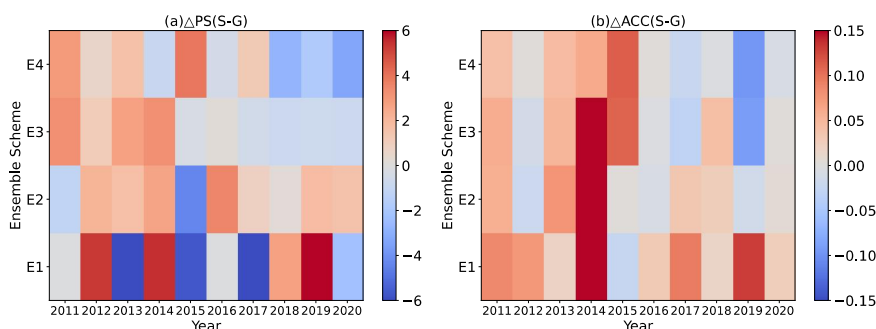
337
 338 **Table 2** 10-year average of RACC and PS score of summer precipitation prediction of
 339 the four UWE in China during 2011 ~ 2020.

Ensemble Scheme	Ensemble member	Grid Ensemble		Station Ensemble	
		RACC	PS	RACC	PS
E1	ORM, GRD	0.04	69.2	0.11	69.3
E2	ORM, GRD, EOF	0.07	69.3	0.11	70.2



E3	ORM, GRD, EOF, REG	0.08	69.9	0.11	70.7
E4	ORM,GRD,EOF,REG,ABN	0.09	70.0	0.10	70.1

340



341

342 **Fig. 3** Scatter distribution of differences of (a) PS and (b) RACC values for UWE of
 343 summer precipitation in China during 2011 - 2020. Values indicates the differences of
 344 station-based ensemble minus the grid-based ensemble.

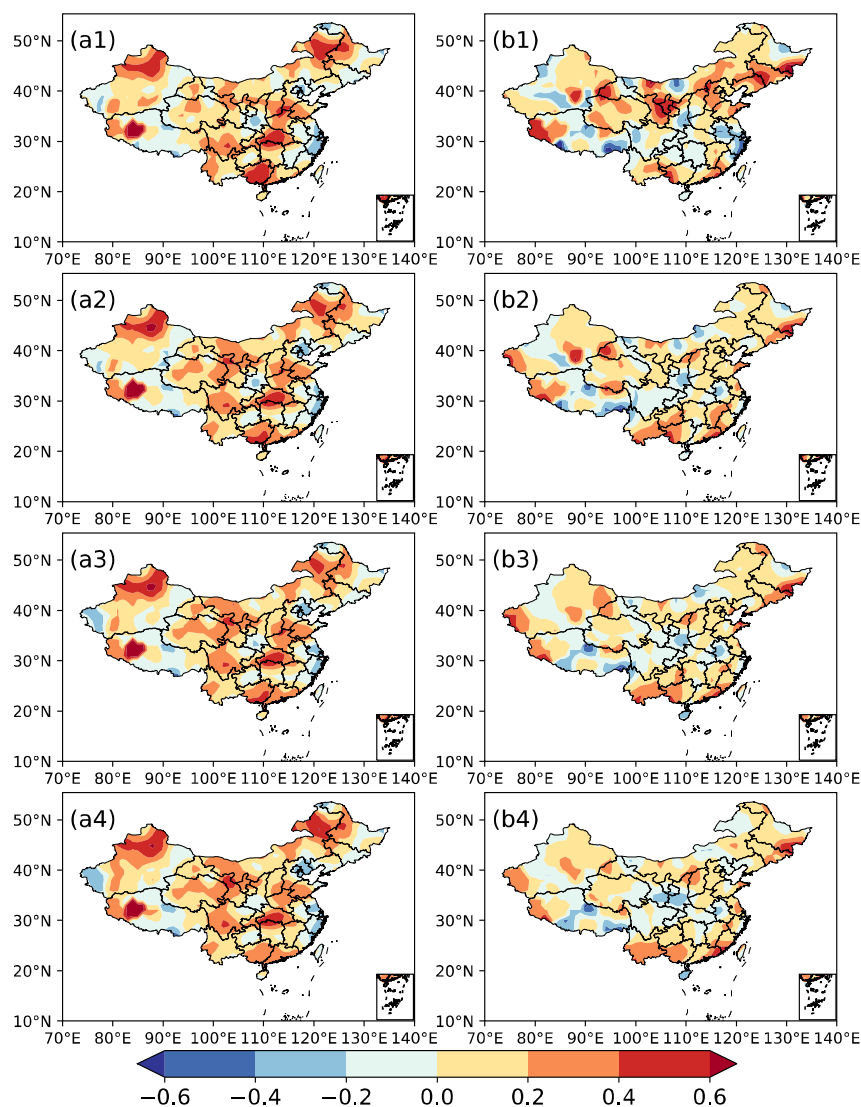
345

346 In Fig. 4, the TCC of the station-based ensemble for summer precipitation prediction
 347 show positive values in most China, with the high value centers distributed in western
 348 South China, central China, southern North China and western Northeast China etc.
 349 The similar spatial distributions are observed in predictions of the four station-based
 350 ensemble schemes (Fig. 4 a, c, e, g). The TCC differences between the station-based
 351 ensemble and the grid-based ensemble indicate that the former has higher than values
 352 than the later in most areas of China, except for part of Central China and East China
 353 (Fig. 4 b, d, f, h). The spatial distribution of TCC indicates the improvement of the
 354 station-based ensemble is suitable for most stations in China and implies this
 355 approach can make the summer precipitation prediction being closer to the
 356 observation. Bueh et al. (2008) also addressed that the training phase of multi-model
 357 ensemble learns from the recent past performances of models and is used to determine
 358 statistical weights from a least square minimization via a simple multiple regression.
 359 During the training process, more precise objective data can produce better weight
 360 coefficients and lead to more accurate ensemble result, which might be the reason for
 361 the station-based ensemble produce better predictions of summer precipitation in
 362 China than the grid-based one.

363 Fig.5 indicates that the probability density distribution of station-based ensemble
 364 predictions is closer to the observation especially at the peak part than the grid-based



365 ensemble and this feature is observed in four ensemble predictions. If the onsite
366 observation dataset can be used for training, we may have a parameterization scheme
367 containing precise information for each single station, which may be of help to
368 produce the prediction being close to the real situation of summer precipitation in
369 China. Since the grid-based dataset normally is the reproduced observation data,
370 which may lose certain precise information especially for those extreme values. This
371 flaw of the grid data may cause it to have poor performance on improving the
372 prediction accuracy than the station data(Kim et al., 2012; Xiong et al., 2011a; Yang et
373 al., 2024).



374

375

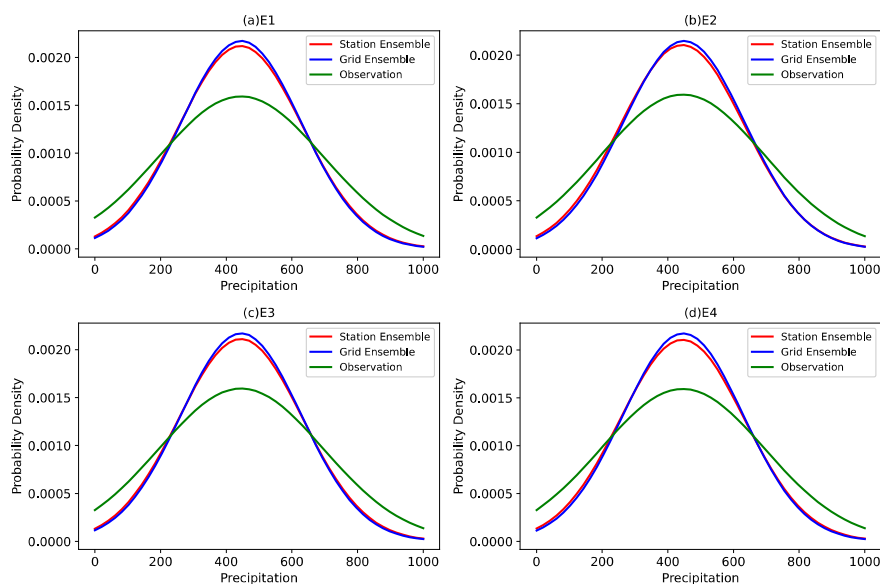
376

377

378

379

Fig. 4 Spatial distribution of TCC of station-based UWE for summer precipitation in China during 2011-2020 (a1-a4), TCC differences of station-based ensemble minus the grid-based ensemble (b1-b4). (a1, b1) Ensemble scheme E1; (a2, b3) Ensemble scheme E2; (a3, b3) Ensemble scheme E3; (a4, b4) Ensemble scheme E4.



380

381 **Fig. 5** Probability density distribution of the total precipitation for observation and
382 UWE. (a) Ensemble Scheme E1, (b) Ensemble Scheme E2, (a) Ensemble Scheme E3,
383 (a) Ensemble Scheme E4.

384

385 **3 Calculating the spatial similarity of ensemble prediction.**

386 In Fig. 6, the SACCs and RACCs are not consistent with each other, and the former
387 are more frequently lower than the latter. The 10-year average values of SACC for
388 each ensemble prediction for summer precipitation in China are also lower than the
389 RACC (table 1). The SACC is calculated after subtracting the spatial average of
390 anomaly for all the stations from the original precipitation anomaly. This approach
391 may cause the new value for each station can't reflect the real situation and lead to a
392 decrease of RACC between the prediction and observation. In fig.7 the correlation
393 between the RACC and PS are all higher than those between the SAAC and PS,
394 which further indicated RACC can better assess the prediction skill of summer
395 precipitation. It is also noted that the differences between the SACC and RACC are
396 quite obvious in 2011 and 2015 for ensemble schemes E2, E3, and E4 (Fig. 6 b, c, d).
397 Comparing with the PS scores, it seems that the RACC for each prediction have more
398 consistent feature than the SACC. In order to figure out if the RACC has the better
399 performance than the SACC on indicating the spatial consistency of precipitation
400 prediction, the observation and prediction of summer precipitation in 2011 and 2015



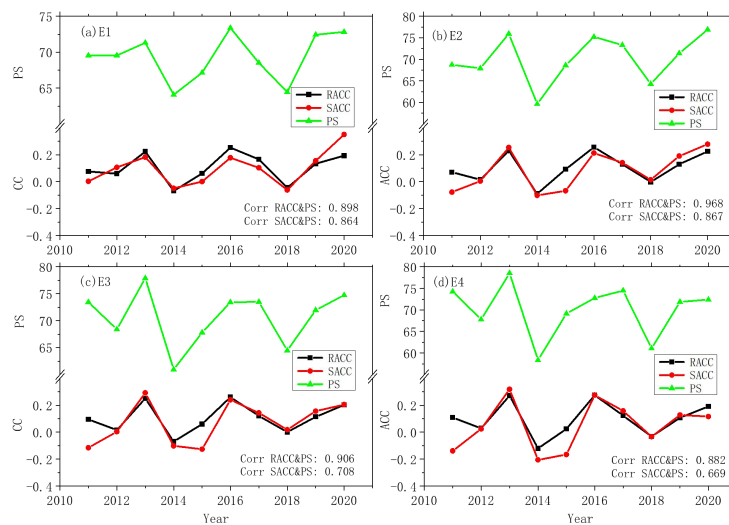
401 are respectively presented in Fig. 7. Comparing with the observation (Fig. 7 a5),
 402 predicted precipitation anomalies in summer 2011 show consistent feature in most
 403 China (Fig. 7 a1-a4). The PS scores of four ensemble schemes are respectively 69.5,
 404 68.7, 73.5, 74.3, and RACCs are 0.08, 0.07, 0.10, 0.11, which properly indicate the
 405 prediction skill of these four predictions on the summer precipitation in 2011. It is
 406 also noted that the SACCs of 2011 prediction are respectively 0.01, -0.08, -0.11 and
 407 -0.14, which obviously have flaws in assessing the performance of these four schemes
 408 on predicting the precipitation. This shortcoming of the SACC is also exhibited in the
 409 prediction of summer precipitation anomalies in 2015 (Fig. 7 b1-b5), owing to its
 410 improperly low SACC values being 0.01, -0.07, -0.13, -0.17, respectively.

411

412 **Table 3** 10-year average of RACC, SACC of station-based ensemble predictions for
 413 summer precipitation in China during 2011-2020.

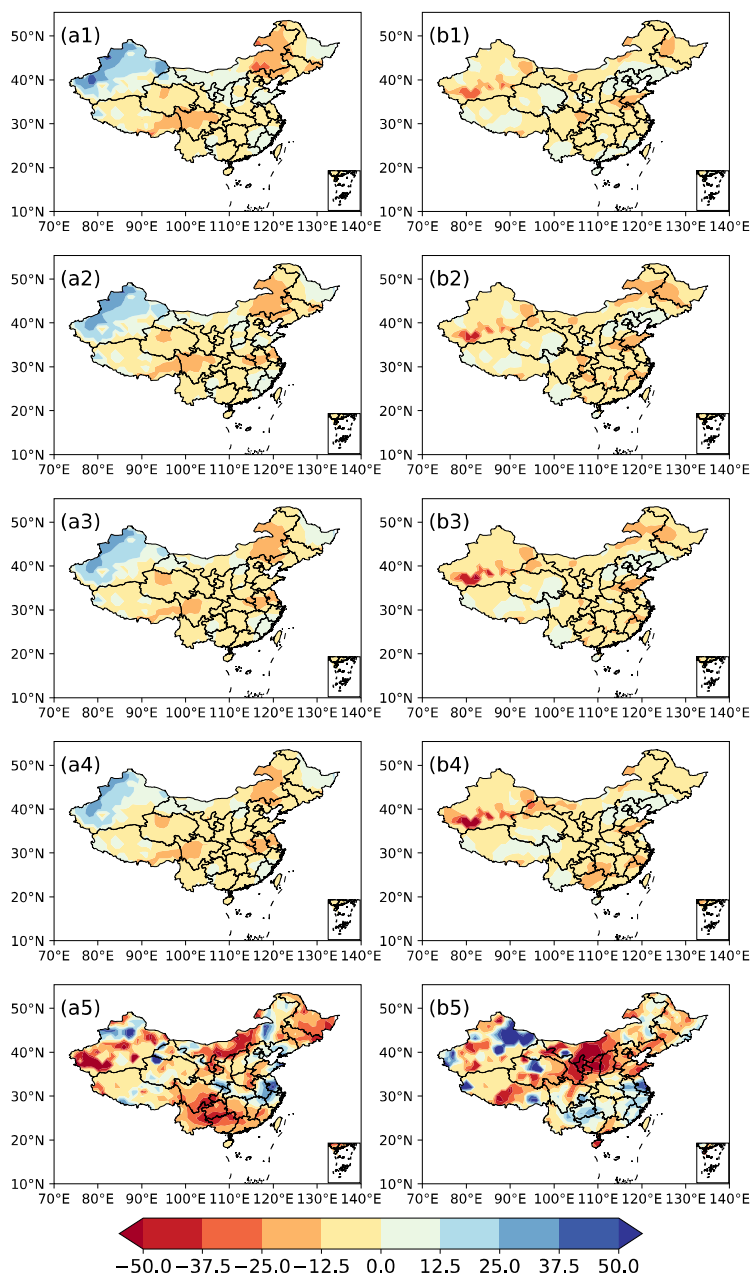
	E1	E2	E3	E4
RACC	0.11	0.11	0.11	0.10
SACC	0.10	0.08	0.07	0.05

414



415

416 **Fig. 6** Annual RACC, SACC and PS of station-based ensemble predictions for
 417 summer precipitation in China. Prediction of (a) E1, (b) E2, (c) E3 and (d) E4
 418 approach, respectively.



419

420 **Fig. 7** The spatial distribution of anomalies (unit: %) of observation and prediction of
421 summer precipitation in 2011 and 2015. (a1-a4) prediction of scheme E1-E4, and (a5)
422 observation for 2011; (b1-b4) prediction of scheme E1-E4, and (b5) observation for
423 2015.



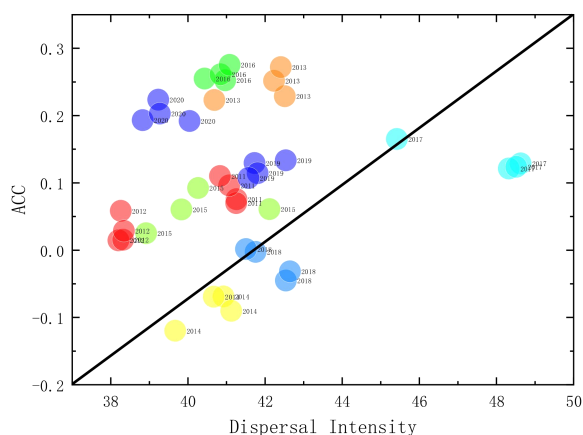
424

425 **4. Impact of dispersal intensity on the ensemble prediction.**

426 The dispersal intensity (Di) also called as the coefficient of variation, which is a
427 variable measure the differences among single samples and can be calculated by
428 formal (5). The dispersal intensity is also a relative measure of variability that
429 indicates the size of a standard deviation in relation to its mean. It is a standardized,
430 unitless measure that allows you to compare variability between disparate groups and
431 characteristics.

432
$$Di = \frac{\sqrt{\sum_{k=1}^n (F_{km} - \bar{F}_m)^2 / n}}{\bar{F}_m} \quad (8)$$

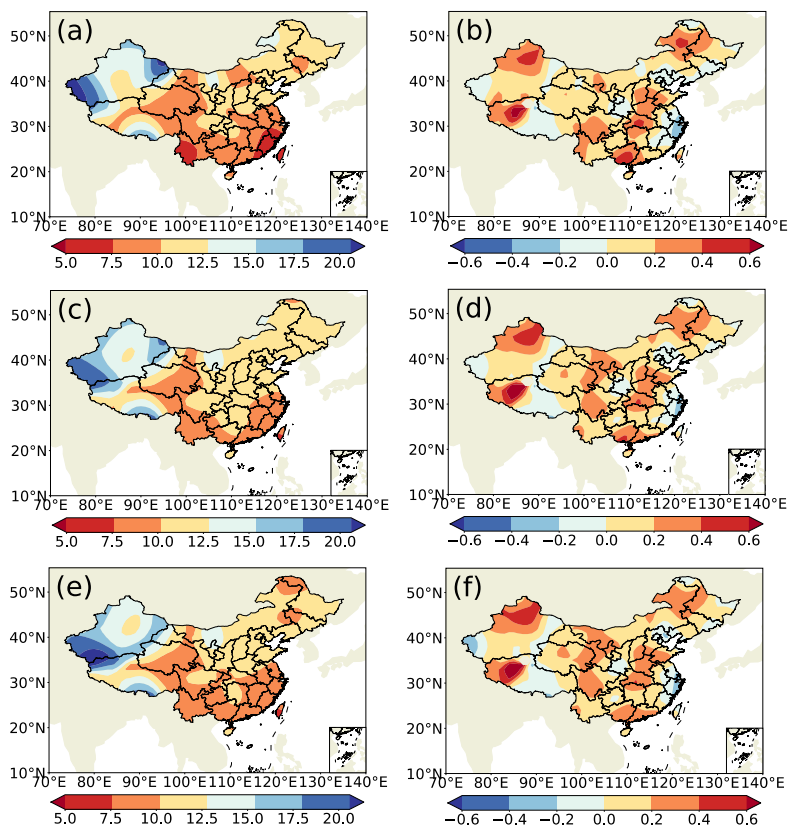
433 Since the dispersal intensity of each statistic-dynamic prediction has obvious
434 interannual variation, it is necessary to analyze its probable impact on the ensemble
435 prediction of summer prediction in China. Fig. 8 presents the relationship of ACC -
436 dispersal intensity of summer precipitation prediction, in which high ACCs of summer
437 precipitation prediction mostly corresponds to the low dispersal intensity among
438 statistic-dynamic predictions. The variabilities of the signal and noise for the
439 ensemble prediction can be measured as the variance of the ensemble mean and
440 ensemble spread of all the initial conditions (Liu et al., 2019; Zheng et al., 2009), the
441 sampling error on measuring the signal variance, the more reasonable estimation of
442 the signal variance can be given and used to measure the overall potential
443 predictability of the prediction system (DelSole, 2004; DelSole and Tippett, 2007).
444 The UWE has the similar theory as the ensemble prediction, the low dispersal
445 intensity among ensemble samples implies the historical similar error selected by
446 different approach is quite closet to each other, which makes the correction on the
447 model prediction is more trustable and then produce a more accurate prediction than
448 those cases with high dispersal intensity.



449

450 **Fig. 8** The relationship between each UME's ACC and the dispersal intensity of each
451 summer precipitation prediction during 2011-2020.

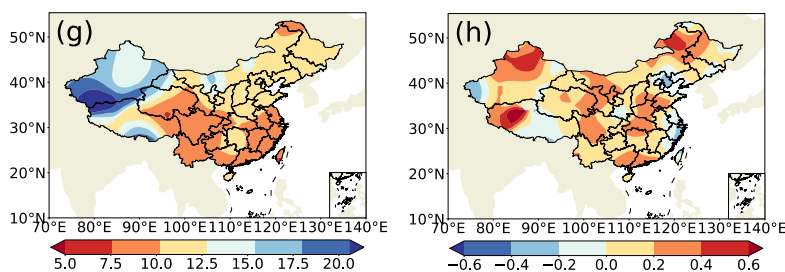
452



453

454

455



456

457

Fig. 9 The spatial distinction of the 10-year average of dispersal intensity (a, c, e, g) and TCC (b, d, f, h) of UME scheme of E1-E4 during 2011-2020.

458

459

460 In Fig. 9, the 10-year average of dispersal intensity of each UME scheme show the
461 similar pattern as the spatial distribution of TCC of summer prediction produced by
462 UME. Except for part of Northwest China and middle East China, the low dispersal
463 intensity also tends to produce high TCC of statistic-dynamic combined ensemble
464 prediction in most China. The low dispersal intensity among the single prediction
465 corresponds to the major physical process captured by each prediction scheme is
466 similar with each other, which is help of the more reasonable estimation of the signal
467 variance and produce the better precipitation predictions.

468

469 5. Conclusions and discussion

470 This study presents the UWE of the dynamic-statistic schemes in order to enhance
471 summer precipitation prediction in China. The analysis also includes an examination
472 of factors that may impact the prediction skill of UWE, such as grid-based and
473 station-based prediction, the calculation of prediction skill, and the influence of
474 sample dispersion on prediction accuracy.

475

476 UWE's performance surpasses the model and the dynamic-statistic scheme predictions,
477 potentially due to its ability to overcome individual model or scheme inadequacies,
478 reduce formulation uncertainties, and yield a more stable and accurate predictions.
479 The average RACC and PS values for the station-based ensemble prediction
480 fluctuated between 0.10-0.11 and 69.3-70.2 from 2011 to 2020, indicating
481 significantly higher proficiency compared to the grid-based ensemble prediction. The
482 ensemble prediction based on station data can produce precipitation with a probability
483 density distribution function that is closer to the observed data compared to the



484 grid-based prediction, making the former more accurate. The use of the SACC needs
485 to remove the spatial average of the whole stations from the original value, which
486 may produce inaccurate station values and lead to a lower correlation between
487 predictions and observations. This makes SACC unsuitable for estimating the spatial
488 consistency of summer precipitation predictions. The commonly used SACC should
489 be supplanted by the updated RACC, which is computed by directly utilizing the
490 precipitation anomalies at each station, without the need to deduct the overall average
491 precipitation anomaly from all stations.

492

493 Moreover, the higher RACCs in summer precipitation prediction are predominantly
494 associated with lower dispersal intensity among the dynamic-statistic predictions.
495 This indicates that a more concentrated ensemble, where predictions are closely
496 aligned, tends to result in more accurate forecasts. Accordingly, the dispersal intensity
497 of ensemble samples is a crucial factor affecting the prediction accuracy of
498 dynamic-statistic combined UWE. UWE shares a similar theoretical foundation with
499 ensemble prediction. Low dispersal intensity among ensemble samples suggests that
500 the historical similar errors identified by various methods are closely aligned. This
501 alignment enhances the reliability of corrections applied to model predictions, thereby
502 yielding more accurate forecasts compared to cases with high dispersal intensities.

503

504 **Acknowledgement.** This work is supported by the National Natural Science Foundation of China
505 Project (Nos.42130610, 42075057, and 42275050) and the National Key Research and Development
506 Program of China (2022YFE0136000).

507

508 **Author contributions.** The conception of this paper is supposed by Xiaojuan Wang and Guolin.
509 Material preparation, data collection, and analysis were performed by Xiaojuan Wang and Zihan Yang.
510 The manuscript is written by Xiaojuan Wang and revised by Qingquan Li. All authors commented on
511 previous versions of the manuscript. All the authors have read and approved the final manuscript.

512

513 **Funding.** The National Natural Science Foundation of China Project (Nos. 42130610, 42075057, and
514 42275050), The National Key Research and Development Program of China (2022YFE0136000).

515 **Data Availability Statement.** The datasets generated during and/or analyzed during the current study
516 are available from the corresponding author on reasonable request.

517 **Ethics declarations.** The authors declare no conflict of interest. Authors have no additional
518 information that might be relevant for the editors, reviewers and readers. The funding sponsors have no



519 participation in the execution of the experiment, the decision to publish the results, nor the writing of
520 the manuscript.

521

522 **Conflict of interest:** The authors have no relevant financial or non-financial interests to disclose.

523

524 **Reference**

525 Bueh C, Shi N, Ji L, Wei J, Tao S (2008) Features of the EAP events on the
526 medium-range evolution process and the mid- and high-latitude Rossby wave
527 activities during the Meiyu period. Chinese Science Bulletin 53:610-623.

528 Candille G (2009) The multiensemble approach: The NAEFS example. Mon.
529 Weather Rev. 137:1655-1665.

530 Chou J (1974) A problem of using past data in numerical weather forecasting (in
531 Chinese). 6:635-644

532 DelSole T (2004) Predictability and information theory. Part I: measures of
533 predictability. J Atmos Sci 61:2425-2440.

534 DelSole T, Tippett MK (2007) Predictability: recent insights from information
535 theory. Rev. Geophys. 45:4002.

536 Ding Y (1994) Monsoons over China. Advances in Atmospheric Sciences.
537 Advances in Atmospheric Sciences 11:252.

538 Ding Y, Li Q, Li W, Luo Y, Zhang P, Zhang Z, Shi X, Liu Y, Wang L (2004) Advance
539 in Seasonal Dynamical Prediction Operation in China. Acta Meteorologica Sinica
540 30:598-612.

541 Fan K, Liu Y, Chen H (2012) Improving the prediction of the East Asian summer
542 monsoon: New approaches. Weather and Forecasting 27:1017-1030.



543 Feng G, Yang J, Zhi R, Zhao J, Gong Z, Zheng Z, Xiong K, Qiao S, Yan Z, Wu Y
544 (2020) Improved prediction model for flood-season rainfall based on a nonlinear
545 dynamics-statistic combined method. *Chaos, Solitons & Fractals* 140:110160.

546 Feng G, Zhao J, Zhi R, Gong Z (2013) Recent progress on the objective and
547 quantifiable forecast of summer precipitation based on dynamical statistical
548 method. *J. Appl. Meteor. Sci* 24:656-665.

549 Gettelman A, Geer AJ, Forbes RM, Carmichael GR, Feingold G, Posselt DJ,
550 Stephens GL, Heever SCvd, Varble AC, Zuidema. P (2022) The future of Earth
551 system prediction: Advances in model-data fusion. *SCIENCE ADVANCES*
552 8:eabn3488.

553 Gong Z, Dogar MMA, Qiao S, Hu P, Feng G (2017) Limitations of BCC_CSM's
554 ability to predict summer precipitation over East Asia and the Northwestern
555 Pacific. *Atmospheric Research* 193:184-191.

556 Gong Z, Hutin C, Feng G (2016) Methods for Improving the Prediction Skill of
557 Summer Precipitation over East Asia–West Pacific. *Weather and Forecasting*
558 31:1381-1392.

559 Gong Z, M. D, Qiao S, P. H, G. F (2018) Assessment and Correction of BCC_CSM's
560 Performance in Capturing Leading Modes of Summer Precipitation over North
561 Asia. *International Journal of Climatology* 38: 2201-2214.

562 Houze RA, Rasmussen JKL, Zuluaga MD, Brodzik SR (2015) The variable nature of
563 convection in the tropics and subtropics: A legacy of 16 years of the Tropical
564 Rainfall Measuring Mission satellite. *Rev. Geophys.* 53:994–1021.



565 Huang G (2004) An Index Measuring the Interannual Variation of the East Asian
566 Summer Monsoon—The EAP Index. *Adv. Atmos. Sci.* 21:41-52.

567 Huang J, Yi Y, Wang S, Chou J (1993) An analogue - dynamical long - range
568 numerical weather prediction system incorporating historical evolution. *Quarterly*
569 *Journal of the Royal Meteorological Society* 119:547-565.

570 Huang R Influence of the heat source anomaly over the tropical western Pacific
571 on the subtropical high over East Asia. in *International Conference on the*
572 *General Circulation of East Asia, Chengdu*, pp. 40-51.

573 Kim H-M, Webster PJ, Curry JA (2012) Seasonal prediction skill of ECMWF System
574 4 and NCEP CFSv2 retrospective forecast for the Northern Hemisphere Winter.
575 *Climate Dynamics* 39:2957-2973.

576 Krishnamurti TN, Kumar V (2012) Improved seasonal precipitation forecasts for
577 the Asian Monsoon using a large suite of atmosphere ocean coupled models:
578 *Anomaly. J. Clim.* 25:65–88.

579 Krishnamurti TN, Kumar V, Simon A, Bhardwaj A, Ghosh T, Ross R (2016) A review
580 of multimodel superensemble forecasting for weather, seasonal climate, and
581 hurricanes. *Reviews of Geophysics* 54:336-377.

582 Lang X, Wang H (2010) Improving Extraseasonal Summer Rainfall Prediction by
583 Merging Information from GCMs and Observations. *Weather and Forecasting*
584 25:1263-1274.



- 585 Li H, Dai A, Zhou T, Lu J (2008) Responses of East Asian summer monsoon to
586 historical SST and atmospheric forcing during 1950–2000. *Climate Dynamics*
587 34:501–514.
- 588 Liu T, Tang Y, Yang D, Cheng Y, Song X, Hou Z, Shen Z, Gao Y, Wu Y, Li X, Zhang
589 B (2019) The relationship among probabilistic, deterministic and potential skills in
590 predicting the ENSO for the past 161 years. *Climate Dynamics* 53:6947–6960.
- 591 Lu RY (2005) Interannual variation of North China rainfall in rainy season and
592 SSTs in the equatorial eastern Pacific. *Chinese Science Bulletin* 50:2069–2073.
- 593 Luo L, Wood EF, Pan M (2007) Bayesian merging of multiple climate model
594 forecasts for seasonal hydrological predictions. *J. Geophys. Res. Atmos.*
595 112:D10102.
- 596 Palmer TN, Alessandri A, Andersen U, Cantelaube P, Davey M, D’el’cluse P,
597 D’equ’e M DiE, Doblas-Reyes FJ, Feddersen H, Graham R, Gualdi S, Gu’er’emy JF,
598 Hagedorn R, Hoshen M, Keenlyside N, LatifM LA, Maisonnave E, Marletto V,
599 Morse AP, Orfila B, Rogel P, Terres J-M, C. TM (2004) Development of a
600 European multimodel ensemble system for seasonal-to-interannual prediction
601 (DEMETER). *Bull. Am. Meteorol. Soc.* 85:853–872.
- 602 Ren HL, Chou JF (2006) Introducing the updating of multi reference states into
603 dynamical analogue prediction. *Acta Meteor. Sinica* 64:315–324.
- 604 Ren HL, Chou JF (2007) Strategy and methodology of dynamical analogue
605 prediction. *Sci. China (D)* 50:1589–1599.



606 Roberts MJ, Hewitt HT, Hyder P, Ferreira D, Josey SA, Mizielinski M, Shelly A (2016)
607 Impact of ocean resolution on coupled air - sea fluxes and large - scale climate.
608 Geophysical Research Letters 43:10,430-410,438.

609 Satoh M, Tomita H, Yashiro H, Miura H, Kodama C, Seiki T, Noda AT, Yamada Y,
610 Goto D, Sawada M (2014) The non-hydrostatic icosahedral atmospheric model:
611 Description and development. Progress in Earth and Planetary Science 1:1-32.

612 Si D, Ding Y (2013) Decadal Change in the Correlation Pattern between the
613 Tibetan Plateau Winter Snow and the East Asian Summer Precipitation during
614 1979–2011. Journal of Climate 26:7622–7634.

615 Specq D, Batté L (2020) Improving subseasonal precipitation forecasts through a
616 statistical–dynamical approach: application to the southwest tropical Pacific. Clim.
617 Dyn. 55:1913–1927.

618 Sun L, Yang X-Q, Tao L, Fang J, Sun X (2021) Changing Impact of ENSO Events
619 on the Following Summer Rainfall in Eastern China since the 1950s. Journal of
620 Climate 34:8105–8123.

621 Tao S (2006) The Westward, Northward Advance of the Subtropical High over the
622 West Pacific in Summer. Journal of Applied Meteorological Science.

623 Vitart F (2006) Seasonal forecasting of tropical storm frequency using a
624 multi-model ensemble. Q. J. R. Meteorol. Soc. 132:647–666.

625 Wang H, Fan K (2009) A New Scheme for Improving the Seasonal Prediction of
626 Summer Precipitation Anomalies. Weather and Forecasting 24:548-554.



627 Wang H, Fan K, Sun J, Li S, Lin Z, Zhou G, Chen L, Lang X, Li F, Zhu Y (2015) A
628 review of seasonal climate prediction research in China. *Advances in Atmospheric*
629 *Sciences* 32:149-168.

630 Wang QJ, Schepen A, Robertson DE (2012) Merging Seasonal Rainfall Forecasts
631 from Multiple Statistical Models through Bayesian Model Averaging. *Journal of*
632 *Climate* 25:5524-5537.

633 Wu J, Vitart F, Wu T, Liu X (2017) Simulations of the Asian summer monsoon in
634 the sub-seasonal to seasonal prediction project (S2S) database. *Quarterly Journal*
635 *of the Royal Meteorological Society* 143:706-727.

636 Wu T, Yu R, Lu Y, Jie W, Fang Y, Zhang J, Zhang L, Xin X, Li L, Wang Z, Liu Y,
637 Zhang F, Wu F, Chu M, Li J, Li W, Zhang Y, Shi X, Zhou W, Yao J, Liu X, Zhao H,
638 Yan J, Wei M, Xue W, Huang A, Zhang Y, Zhang Y, Shu Q (2021) BCC-CSM2-HR:
639 A High-Resolution Version 1 of the Beijing Climate Center Climate System Model.
640 *Geoscientific Model Development* 14:2977-3006.

641 Xiong K, Feng G, Huang J, Chou J (2011a) Analogue-dynamical prediction of
642 monsoon precipitation in Northeast China based on dynamic and optimal
643 configuration of multiple predictors. *Acta. Meteor. Sin.* 25:316-326. .

644 Xiong KG, Feng GL, Huang JP, Huang JF (2011b) Analogue-dynamical prediction
645 of monsoon precipitation in Northeast China based on dynamic and optimal
646 configuration of multiple predictors. *J. Meteor. Sci* 25:316-326.



647 Yan X, Tang Y (2013) An analysis of multi-model ensembles for seasonal climate
648 predictions. Quarterly Journal of the Royal Meteorological Society 139:
649 1179-1198.

650 Yang J, Zhao J, Zheng Z, Xiong KG, Shen B (2012) Estimating the Prediction Errors
651 of Dynamical Climate Model on the Basis of Prophase Key Factors in North China.
652 Chin. J. Atmos. Sci. 36:11-22.

653 Yang Z, Bai H, Tuo Y, Yang J, Gong Z, Wu Y, Feng G (2024) Analysis on the
654 station-based and grid- based integration for dynamic-statistic combined
655 predictions. 155:5184.

656 Zheng F, Wang H, Zhu J (2009) ENSO ensemble prediction: Initial error
657 perturbations vs. model error perturbations. Chinese Science Bulletin
658 54:2516-2523.

659 Zhu J, Shukla J (2013) The Role of Air–Sea Coupling in Seasonal Prediction of
660 Asia–Pacific Summer Monsoon Rainfall. Journal of Climate 26:5689-5697.
661
662